THE JOURNAL OF PHYSICAL CHEMISTRY C
A JOURNAL OF THE AMERICAN CHEMICAL SOCIETY

pubs.acs.org/JPCC
Article

Commensurability of Monolayer Silica on Cu(111)

Tim Kratky, Paul Leidinger, Francesca Genuzio, Tevfik Onur Menteş, Andrea Locatelli, and Sebastian Günther*

Cite This: J. Phys. Chem. C 2024, 128, 7235−7241
Read Online

ACCESS | Metrics & More | Article Recommendations

ABSTRACT: We report a combined low-energy electron and X-ray photoemission electron microscopy (LEEM/XPEEM) study on the formation of monolayer silica by oxygen-induced segregation of bulk dissolved silicon on a (111)-textured Cu foil. The structure forms on Cu foils, on which graphene was previously grown by chemical vapor deposition (CVD) in a quartz tube reactor. The CVD reactor treatment transforms the initial polycrystalline into a (111)-textured Cu foil but also initiates the bulk dissolution of released silicon. After prolonged oxygen dosing, XPEEM proves the formation of micrometer-sized silica islands, which remain the exclusive surface layer after burning the covering graphene layer. LEEM data acquired from the silica islands delivers a diffraction pattern identical to the one reported for monolayer silica prepared by Si evaporation in the presence of oxygen on preoxidized Cu(111). The diffraction pattern analysis identifies the appearing *k*-space frequencies as the ones of a moiré pattern and proves the commensurability of the silica layer on the Cu(111) support. The commensurate structure appears for a 30° rotated silica lattice with the lattice constant of $a[SiO_x]$ = 5.15 Å leading to a (7×7) unit cell of the Cu(111) support hosting a $(2\sqrt{3} \times 2\sqrt{3})R_{30°}$ cell of the silica lattice. In our analysis, all possible moirés at a rotation angle of 30° are deduced for the case of SiO_x on Cu(111) and it is explained why the observed moiré structure appears. The performed moiré analysis may be applied for many 2-dimensional materials and especially for silica on other hexagonally packed transition metals. The fact that the commensurate surface silica phase can be locally prepared without preoxidation of Cu(111) is discussed.

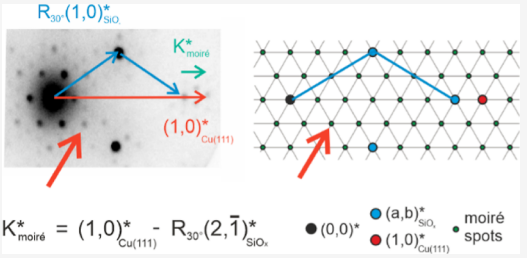

INTRODUCTION

Thin oxide films can serve as support surface for model catalysts and have thus been investigated for decades.[1] Well-ordered thin oxides may also be synthesized heteroepitaxially and provide the oxide support in a variety of catalytic platforms with examples including alumina, titania, ceria, vanadia, etc. and silica thin films.[2−5] Monolayer silica has been already successfully synthesized on a variety of metal surfaces where it arranges as distorted and more-or-less defective honeycomb lattice leading either to an amorphous[6,7] or to a crystalline overlayer.[8−12] In the latter case, the matching condition with the substrate lattice determines whether the overlayer is commensurate or incommensurate. Recently, the preparation of monolayer silica on Cu(111) was reported.[13] The preparation relied on the preoxidation of Cu(111) and the subsequent evaporation of silicon in the presence of O_2. A well-ordered single-layer silica film was achieved with the silica lattice rotated by 30° with respect to the Cu(111) support lattice. The overlayer was considered as incommensurate which was also stated by Xu et al. in a later study.[14]

Using an alternative path for silica growth, here, we show that monolayer silica forms a commensurate structure on Cu(111). In particular, we use the silicon contamination from the quartz tube reactor during the CVD synthesis of graphene on copper as the silicon source. Silica formation on Cu plays a role during chemical vapor deposition (CVD) of graphene on Cu foils in quartz tube reactors where silicon is a known contaminant.[15−19] Special pretreatments performed in a quartz glass reactor prior to the actual CVD synthesis convert the polycrystalline Cu foils into a (111)-textured support.[20−22] As will be shown elsewhere, such preparation procedures are capable of introducing Si originating from the quartz tube walls to the Cu foil bulk. Subsequent exposure of the Cu foil to oxygen induces the segregation of Si to the foil surface and the local formation of SiO_x islands.[23]

In this work, we use X-ray photoemission electron microscopy (XPEEM), low energy electron microscopy (LEEM), and microspot low energy electron diffraction (*μ*-LEED) to show that these islands are structurally identical to the monolayer silica reported in the literature proving an alternative path to the surface silica phase by Si segregation.[13,14] A detailed *k*-space frequency analysis of the moiré pattern in comparison to the diffraction spots observed in

Received: December 22, 2023
Revised: April 3, 2024
Accepted: April 4, 2024
Published: April 19, 2024

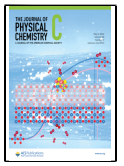

LEED proves the commensurability of the silica layer with the underlying Cu(111) support. The moiré analysis identifies all possible commensurate phases of a 30° rotated silica lattice on Cu(111). It is argued why the commensurate phase leads to a (7×7) unit cell of the Cu(111) support hosting a $(2\sqrt{3} \times 2\sqrt{3})R_{30°}$ cell of the silica layer. The outlined moiré analysis is readily applied for any 2-dimensional material on a hexagonally packed support. Moreover, the gained insight into the formation of ultrathin silica on Cu(111) will influence the understanding of CVD syntheses carried out in quartz tube reactors. It may also be of importance in the field of heterogeneous catalysis whenever transition metals come into contact with silicon-containing species.

METHODS

The experiments were performed at the Nanospectroscopy beamline of the Elettra synchrotron facility making use of the spectroscopic photoemission and low energy electron microscope (SPELEEM) described elsewhere.[24,25] The monolayer silica film was formed on a Cu foil, on which graphene flakes were synthesized by CVD in a quartz tube reactor. Details of the silica formation process will be outlined in a separate publication.[23]

The sample preparation procedure is summarized as follows: prior to the actual CVD graphene growth, the polycrystalline Cu foil was annealed at 945 °C (heating ramp = 20 K/min) in an O_2/Ar atmosphere [p(total) = 12 mbar, O_2/Ar = 1:15,000] for 45 min and then at 1045 °C for 1 h. The subsequent reduction in pure hydrogen at $p(H_2)$ = 300 mbar for 160 min induced the formation of a Cu(111) textured foil in accordance with preparation recipes reported in the literature.[20−22] As outlined in ref 26 and described in ref 23, the Cu foil pretreatment induced Si dissolution in the Cu foil bulk before graphene flakes were synthesized by CVD at T = 1045 °C [$p(H_2)$ = 20 mbar, $p(CH_4) = 2 \times 10^{-2}$ mbar] for 20 min. Subsequent to graphene growth, the sample was rapidly cooled to room temperature in less than a minute, removed from the quartz tube reactor, and exposed to air for 2 weeks prior to analysis at the Nanospectroscopy beamline at Elettra. After insertion in the ultrahigh vacuum chamber of the SPELEEM instrument, the sample was gently degassed in steps of 50 °C up to 250 °C (total degassing time 10 h) and imaged in situ during annealing and oxygen exposure. Upon dosing 600 L O_2 at a temperature between 600 and 650 °C, the graphene film inhibited any O_2 adsorption apart from defects, such as wrinkles in the graphene layer. As a result, oxygen adsorption took place exclusively along these defects, where it segregated the dissolved Si and locally formed a surface silica phase. Due to the restricted oxygen adsorption along wrinkles in the covering graphene layer, the sample develops a surface structure at the mesoscopic length scale. Additional dosing of 900 L O_2 at 700 °C finally removed the graphene layer by oxidation leading to a clean Cu(111) surface partially covered by the formed silica islands.

RESULTS AND DISCUSSION

Figure 1 provides the chemical and structural characterization of silica islands hosted on a (111)-textured Cu foil surface by LEEM, XPEEM, and μ-LEED, along with a comparison to LEED data published in ref 13.

Figure 1a reproduces electron diffraction patterns at 78 and 110 eV from the work of Navarro et al.[13] The silica films were synthesized by silicon evaporation on preoxidized Cu(111) in the presence of gas phase oxygen. The data indicate the reciprocal vectors of the silica lattice which are visible at 78 and 110 eV (green circles), whereas the first-order Cu(111) reciprocal lattice spots appear at 110 eV only (black circles). Figure 1b displays the LEEM image of a (111)-textured polycrystalline Cu foil which contained Si in the bulk that was segregated to the surface by oxygen dosing at temperatures up to 700 °C (total dosing of 1500 L—see Methods Section).[23] The image, acquired at a field of view (FOV) of 15 μm, displays micrometer-sized bright islands nucleated along lines on the polycrystalline Cu surface, which appears dark in the LEEM image when not covered by islands. The orange dashed circle indicates the region where imaging X-ray photoelectron spectroscopy data were recorded by XPEEM. Figure 1c shows the XPEEM data together with the local core level spectra from the bright islands and surrounding Cu foil. Insets display images that reflect the yield of emitted photoelectrons released from the O 1s, Si 2p, and Cu 3p core levels at X-ray energies of 650, 200, and 400 eV, respectively. The identified O 1s and Si 2p peak positions at about 532 and 103 eV, respectively, and the O 1s peak shape are in fair agreement with XPS data reported by Xu et al. for thin silica films on Cu(111) which were synthesized by Si evaporation in the presence of oxygen on preoxidized Cu(111).[14] Thus, the O 1s, Si 2p, and Cu 3p data identify the bright islands of Figure 1b as surface silica on copper. In contrast, silicon and oxygen are absent on dark Cu foil areas uncovered by the islands. The Cu 3p photoelectron emission signal is attenuated by about 20% due to the silica islands on top. This level of attenuation for 325 eV photoelectron kinetic energy is consistent with a silica thickness of a single monolayer.[27,28]

Figure 1d compiles local electron diffraction patterns acquired at the indicated positions in Figure 1b (blue, red, and green circles). The hexagonal pattern taken from the uncovered part identifies the bare Cu foil surface as Cu(111) with the first-order Cu lattice spots at the edge of the imaged k-space (see blue circle). The electron diffraction pattern obtained from the silica islands (red circle) contains moiré spots similar to those reported in the literature (see Figure 1a).[13,14] The presence of the well-resolved diffraction pattern indicates the formation of a single crystalline phase on the entire area covered by the micrometer-sized islands without symmetry-breaking rotational domains in the surface layer. The sharp spot sizes also evidence that other defects such as translational domain boundaries do not occur at a density that limits the coherent domain sizes to a value lower than the transfer width of the instrument. Comparison with the blue-framed diffraction pattern confirms that the $(1,0)^*_{Cu(111)}$ and symmetrically equivalent spots appear as weak satellites in the red-framed diffraction pattern of the silica islands. This fact becomes obvious when irradiating an area hosting both phases in coexistence, as shown in the green-framed LEED pattern.

Having identified the first-order lattice vectors of both lattices, we can index the LEED diffraction spots in Figure 2. The magnified k-space region shows that the rotation of the silica layer by 30° with respect to the Cu(111) lattice induces a moiré vector $K^*_{moiré}$ along the $[1,0]^*_{Cu(111)}$ direction. As sketched in Figure 2, the indicated k-space vectors lead to eq 1

$$K^*_{moire} = (1, 0)^*_{Cu(111)} - R_{30°}(2, \bar{1})^*_{SiO_x} \quad (1)$$

https://doi.org/10.1021/acs.jpcc.3c08360
J. Phys. Chem. C 2024, 128, 7235−7241

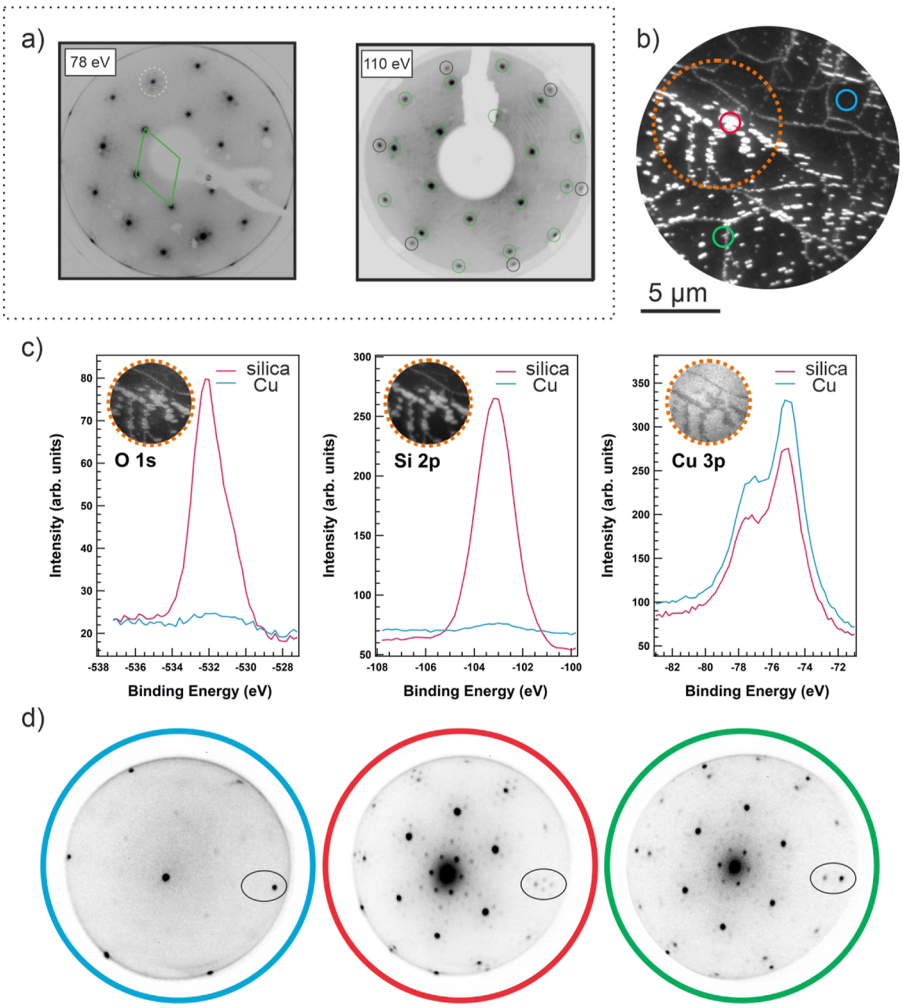

Figure 1. (a) LEED patterns acquired at 78 eV and 110 V from monolayer silica synthesized on preoxidized Cu(111). (Reproduced from ref 13. Copyright [2020] American Chemical Society.) (b) LEEM image (electron energy 40 eV, FOV = 15 μm) showing silica islands (bright) surrounded by an uncovered Cu foil surface (dark) obtained by the preparation described in the Methods section. An orange dotted circle indicates the region where XPEEM data were acquired and small colored circles where μ-LEED data were taken. (c) XPEEM data identifying the islands as silica on bare Cu (O 1s taken at 650 eV, Si 2p at 200 eV, and Cu 3p at 400 eV photon energy, imaged FOV = 7.5 μm). (d) μ-LEED data acquired at 40 eV at the positions indicated in (b). Blue: dark area = bare Cu(111) surface. Red: bright patches = silica islands. Green: Cu foil area including both phases. An ellipse indicates the *k*-space position where the first-order diffraction spots of the Cu(111) lattice and the silica overlayer appear.

According to the nomenclature introduced in ref 29, the acquired diffraction pattern of silica on Cu(111) relates to a second-order moiré. Conversion from reciprocal to real space leads to the length of the moiré vector given by eq 2

$$L_{\text{moire}} = m \times a[\text{Cu}(111)] = n/\sqrt{3} \times a[\text{SiO}_x] \quad (2)$$

In the case of m and n being integer numbers, the structure is commensurate. The possible solutions of eq 2 are visualized in the commensurability plot shown in Figure 2 (bottom). The vertical axis represents the silica lattice constant, and the horizontal one represents the values of the integer number n that refers to the silica lattice (vertical blue lines). Red curves display the respective solution of eq 2 for given m-values between 1 and 24 as a function of the silica lattice constant. Where vertical blue lines and red curves cross, commensurability is met at the given silica lattice constant. Such cases are indicated by green circles. It is evident that the number of commensurate phases increases with increasing n-value, i.e., with increasing moiré length. The redundant commensurate moirés are indicated by dashed green circles and relate to multiples of identified smaller unit cells.

The displayed range of silica lattice constants between 5.0 and 5.5 Å spans the region where thin SiO_x films were observed on other supports. Table 1 compiles several reported cases with silica lattice constants of $a[\text{SiO}_x] > 5.1$ Å.

Note that $a[\text{SiO}_x] < 5.10$ Å is unlikely for silica films on Cu(111) as it would require an unphysical compression of silica at a turning angle of 30° to fit the underlying Cu(111) substrate ($a[\text{Cu}(111)] = 2.55$ Å), while it would have matched already the substrate lattice at $a[\text{SiO}_x] = 5.10$ Å in aligned registry with a (2 × 2) unit cell. Three cases for the smallest possible moirés appear in the commensurability plot, with the third one referring to a moiré with $a[\text{SiO}_x] < 5.10$ Å. The first two small n-value moirés are indicated by a dashed and a solid arrow in Figure 2 (bottom). The respective moirés deliver a commensurate cell with a (6 × 6) or (7 × 7) unit cell when indexing with respect to the Cu(111) substrate. The magnified *k*-space region of the LEED pattern and the commensurability plot of Figure 2 are repeated in Figure 3a together with the

https://doi.org/10.1021/acs.jpcc.3c08360
J. Phys. Chem. C 2024, 128, 7235−7241

Table 1. Reported Structures and Lattice Constants of Supported Thin Silica Films

support	structure	silica lattice constant $a[SiO_x]$	references
Ru(0001)	(2×2) at room temperature	5.42 Å	Yang et al.[7]
	(10×10) after annealing to 1070 K	5.23 Å	
Ru(0001)	(2×2)	5.4 Å	Kremer et al.[12]
Mo(112)	$c(2 \times 2)$	5.2 Å along $[\bar{3}11]$	Weissenrieder et al.[9]
		5.5 Å along $[\bar{1}\bar{1}1]$	
Mo(112)	$c(2 \times 2)$	5.2 Å	Schroeder et al.[8]
			Chen and Goodman[5]
SiC(000$\bar{1}$)	$(\sqrt{3} \times \sqrt{3})R_{30°}$	5.3 Å	Tochihara et al.[30]
Pt(111)	(2×2)	5.54 Å	Yu et al.[10]
Pd(100)	$\begin{pmatrix} 2 & 0 \\ -1 & \sqrt{3} \end{pmatrix}$	5.50 Å	Altman et al.[11]

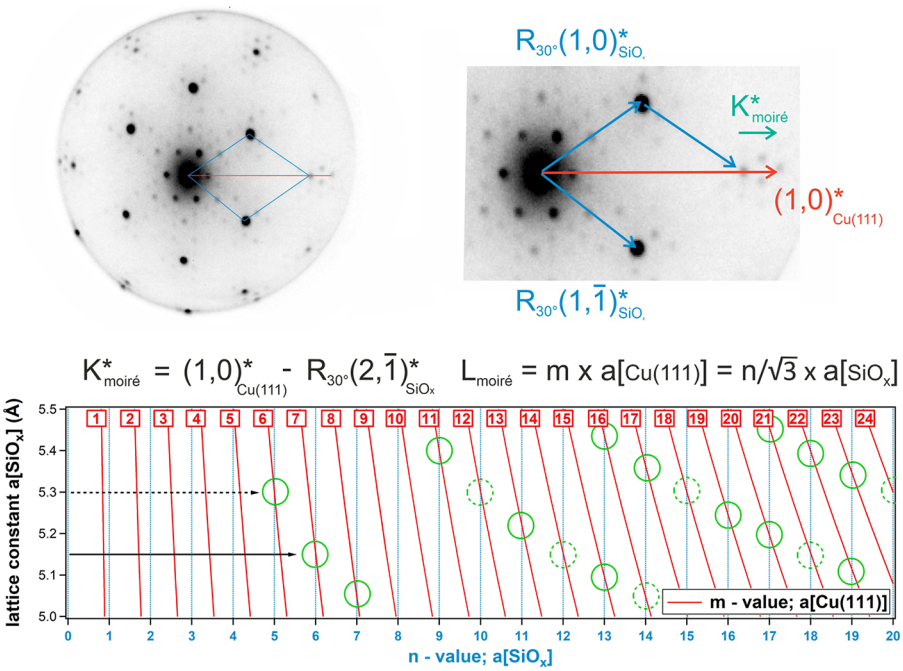

Figure 2. Top row: μ-LEED pattern and magnified region around the (0,0)* spot acquired from the silica island on Cu(111) at 40 eV (see Figure 1d, red frame). The indexed k-space vectors lead to the derivation of the reciprocal moiré vector $K^*_{moiré}$ (see eq 2). Conversion to real space gives the length of the moiré vector $L_{moiré}$. Bottom: commensurability plot indicating the possible commensurate moiré patterns at a rotation angle of the silica layer with respect to the Cu(111) substrate lattice by 30°. Solid and dashed black arrows indicate the solution of eq 2 with the smallest possible moiré length (see text).

moiré frequency analysis of these two cases as sketched in Figure 3b,c, respectively. It will be shown below that the silica film on Cu(111) delivers the moiré frequencies displayed in Figure 2c.

The center panel of Figure 3b displays all moiré frequencies (small green spots) occurring for the case of a silica lattice (blue spots) with $a[SiO_x]$ = 5.30 Å at a rotation angle of 30° with respect to the Cu(111) substrate (red spots), which originate from spatial beating frequencies up to the second order. As indicated in the commensurability plot in real space and as seen also in k-space in Figure 3b, the commensurate cell appears at integer numbers m = 6 and n = 5, i.e., where 5 moiré units match the (2,1)* vector of the silica lattice and 6 moiré units the (1,0)* vector of the Cu lattice. However, when using the $K^*_{moiré}$ vectors close to the origin at (0,0)* (black spot) to span a grid in k-space, one sees that not all second-order moiré spots hit the crossing points of this grid. This becomes even more evident when plotting all appearing eighth order spatial frequencies (see right panel of Figure 3b) which fill a complete lattice in k-space; i.e., each spot resides on a grid. However, this grid is three times smaller in k-space than the one spanned by the calculated vectors $K^*_{moiré}$. It was shown that in such a case, the commensurate moiré relates to a three times augmented cell in real space hosting three moiré frequencies per unit cell with a cell length that is $\sqrt{3}$ times larger than the number calculated by eq 2.[31]

Diffraction peaks of a LEED pattern can be directly related to spatial moiré frequencies in k-space based on the close relationship between multiple scattering in electron diffraction and moiré frequencies.[31,32] For illustration purposes, we plot the eighth order moiré spots in a separate sketch in the left panel of Figure 3b which corresponds to the k-space region of Figure 3a. Here, four additional moiré spots are predicted along the radial direction between the (0,0)* and (1,0)* spots of the silica layer. Halfway between (0,0)* and (1,0)*, no moiré spot should appear which also holds for symmetrically equivalent spots in contrast with the experimental observation of LEED spots precisely at these positions as marked by the

https://doi.org/10.1021/acs.jpcc.3c08360
J. Phys. Chem. C 2024, 128, 7235−7241

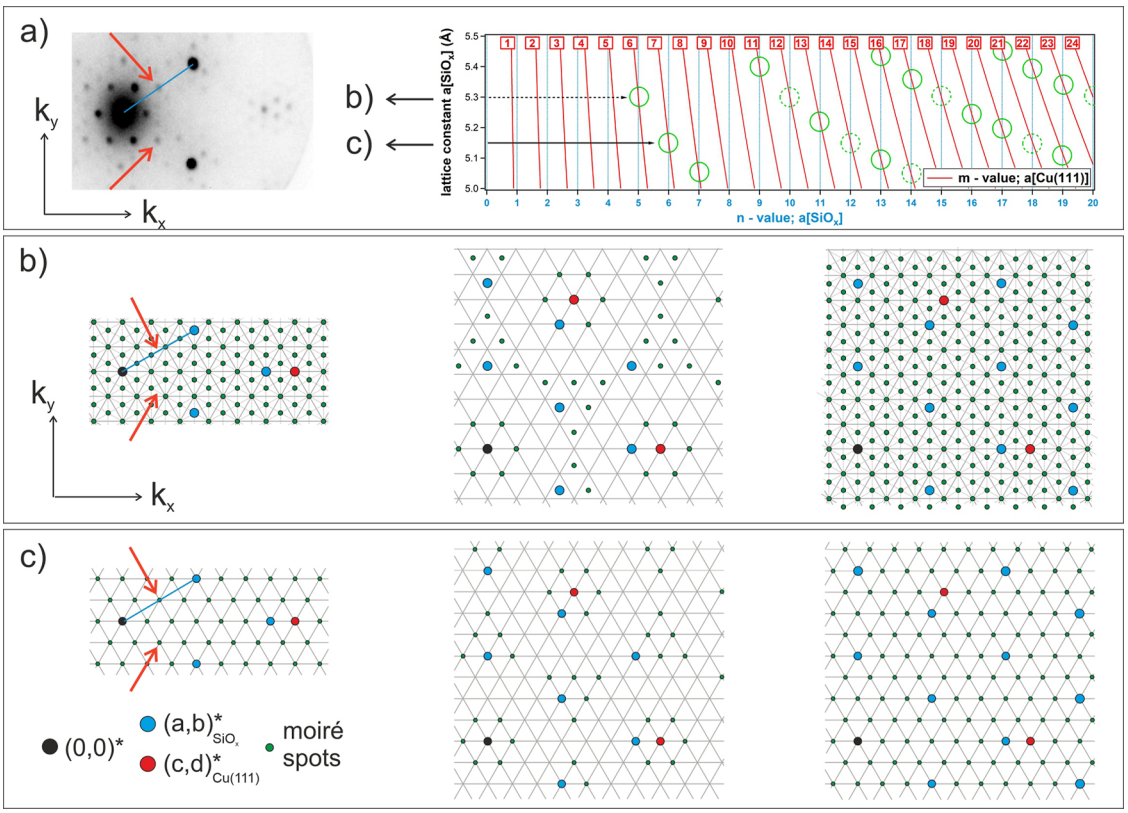

Figure 3. (a) Magnified *k*-space region of the diffraction pattern of silica/Cu(111) and the commensurability plot for a 30° rotated silica lattice on top of Cu(111) leading to the low *n*-value moirés (b,c). The spatial frequency analysis of the respective moirés with silica lattice constants of 5.30 and 5.15 Å is sketched for second (center panels) and eighth order moiré frequencies (right panels) in (b,c), respectively (see text). The panels on the left side display the respective eighth order moiré in a magnified *k*-space region corresponding to the diffraction pattern shown in (a). They highlight moiré frequencies, appearing along the $[1,0]^*_{SiO_x}$ direction. Red arrows point to positions symmetrically equivalent to halfway between the $(0,0)^*$ and the $(1,0)^*_{SiO_x}$ spot where a peak is absent in the case of (b) and present in the case of (c). Considering the clear observation of diffraction spots in the marked positions, it can be concluded that the moiré (c) with a silica lattice constant of 5.15 Å is realized by nature (see text).

red arrows in Figure 3a,b. Thus, we rule out the $a[SiO_x]$ = 5.30 Å moiré, as it is incompatible with the experimental data. Note that the commensurate moiré relating to m = 8 and n = 7 for the improbable case of $a[SiO_x]$ < 5.1 Å also refers to such a case with a tripled cell showing no spot at the indicated position. In the corresponding panels of Figure 3c, we repeat the same analysis for the commensurate case with integer numbers m = 7 and n = 6 and a silica lattice constant of $a[SiO_x]$ = 5.15 Å. The appearing second and eighth order moiré spots plotted in the center and right panel look similar to the moiré frequencies shown in Figure 3b. However, in contrast to the case of Figure 3b, the $K^*_{moiré}$ vectors now span a grid in *k*-space that hosts every appearing moiré spot. As a result, Figure 3c displays a moiré where $L_{moiré}$ calculated from eq 2 represents the length of a unit cell that hosts a single moiré beat per cell. For the lattice constant of $a[SiO_x]$ = 5.15 Å, this equals a (7 × 7) unit cell when referring to the Cu substrate which coincides with a $(2\sqrt{3} \times 2\sqrt{3})R_{30°}$ cell of the 30° rotated silica lattice.

Summing up the above-stated arguments, the $(7 \times 7)/(2\sqrt{3} \times 2\sqrt{3})R_{30°}$ moiré is the smallest possible simple cell for the silica layer on top of the Cu(111) substrate. The moiré spots plotted in the zoomed area of the left panel also match the diffraction spots of the observed LEED pattern with a pronounced diffraction peak at halfway between the $(0,0)^*$ and the $(1,0)^*_{SiO_x}$ spot (see red arrow). Thus, the case shown in Figure 3c with a silica lattice constant of $a[SiO_x]$ = 5.15 Å is identified as being realized by nature.

Since the satellite spots appearing in the diffraction pattern of Figure 1a (acquired by Navarro et al.) are compatible with the spot positions observed by us (see Figure 1d), both silica phases have the same structural properties. Following the moiré analysis outlined in Figures 2 and 3, we conclude that the monolayer silica phase synthesized by Si evaporation on preoxidized Cu(111) reflects a commensurate surface structure in contrast to the claimed incommensurability. Indeed, the calculated length of the $(7 \times 7)/(2\sqrt{3} \times 2\sqrt{3})R_{30°}$ moiré with $L_{moiré}$ = 17.85 Å matches their DFT model and is also connected to the contrast of the silica phase as imaged by scanning tunneling microscopy (STM).[13] The authors identified a superstructure with a cell length of 3 nm along the main axis of the topmost silica lattice. This number amounts to $\sqrt{3} \times 7 \times a[Cu(111)]$ and corresponds to a tripled cell, 30° rotated with respect to the smaller, 17.85 Å moiré cell. In fact, close inspection of the STM data reveals contrast caused by the smaller moiré cell with a wavelength of $L_{moiré}$ = 17.85 Å. Thus, all observed contrast features resolved by STM in addition to the acquired diffraction data can be understood as beating frequencies of a commensurate silica honeycomb lattice on top of Cu(111). It may be that the intercalated oxygen layer of the preoxidized Cu(111) surface adds to the contrast observed in STM but the much simpler beating of a commensurate silica lattice on Cu(111) already

https://doi.org/10.1021/acs.jpcc.3c08360
J. Phys. Chem. C 2024, 128, 7235−7241

suffices to explain the obtained data. However, DFT calculations supported an energetically stabilizing effect of an oxygen layer below the synthesized monolayer silica. I.e., the preoxidation of Cu(111) energetically stabilizes the formation of the silica layer by the intermediate surface oxide layer between the silica and the Cu(111) lattice. These findings are in line with the preparation sequence through Si evaporation on top of a preprepared Cu-oxide interface layer.

In our study, silica formation proceeded through the segregation of Si dissolved in the Cu bulk. In the case of an already formed surface Cu-oxide layer, Si atoms from the Cu bulk would have to penetrate the oxide layer without using the surface oxygen atoms for the formation of Si−O bonds. Alternatively, the Si−O bonds might form immediately when Si atoms approach the Cu surface, but then, the Cu-oxide layer at the interface needs to grow afterward upon further oxygen dosing. In the latter case, the adsorbing oxygen atoms would have to penetrate the topmost silica layer or intercalate by lateral diffusion underneath. Such scenarios seem less likely.

Although our findings do not prove or contradict that the Cu-oxide interface is required for the formation of the surface silica phase, we can state, based on our XPEEM/LEEM data, that both the Si evaporation and the Si segregation route lead to silica with a commensurate honeycomb lattice of same lattice constant and orientation with respect to the underlying Cu(111) support. As stated by Navarro et al., the Cu-oxide layer on top of Cu(111) is prepared in the Si evaporation synthesis route to inhibit Si and Cu intermixing and provide the oxygen atoms for silica formation.[13] Thus, this interface might also act as a Si diffusion barrier during synthesis, which is required for clean Cu(111) but not on already Si-loaded supports.

CONCLUSIONS

In summary, surface segregation of bulk Si upon oxygen exposure at 700 °C was shown to lead to the formation of silica on a (111)-textured Cu foil. Electron diffraction and XPEEM data proved that this segregated silica layer seems to be identical to the synthesized silica film on oxygen precovered Cu(111) reported in the literature.[13,33] A detailed moiré frequency analysis of electron diffraction data identified a commensurate phase with a (7×7) unit cell of the Cu(111) support hosting the $(2\sqrt{3} \times 2\sqrt{3})R_{30°}$ cell of the rotated silica lattice. Thus, preparation of the silica film introducing Si from above the Cu surface (evaporation) or from below (segregation) leads to silica with the same honeycomb lattice constant and orientation on the Cu(111) support. The outlined general LEED data analysis can be applied to any structural characterization of supported ultrathin materials.

AUTHOR INFORMATION

Corresponding Author

Sebastian Günther − *Department of Chemistry, Physical Chemistry with Focus on Catalysis, Technical University of Munich (TUM), 85748 Garching, Germany; Catalysis Research Center, 85748 Garching, Germany;* orcid.org/0000-0002-2415-232X; Email: sebastian.guenther@tum.de

Authors

Tim Kratky − *Department of Chemistry, Physical Chemistry with Focus on Catalysis, Technical University of Munich (TUM), 85748 Garching, Germany; Catalysis Research Center, 85748 Garching, Germany;* orcid.org/0000-0002-8402-6640

Paul Leidinger − *Department of Chemistry, Physical Chemistry with Focus on Catalysis, Technical University of Munich (TUM), 85748 Garching, Germany; Catalysis Research Center, 85748 Garching, Germany;* Present Address: Paul Scherrer Institut, 5232 Villigen PSI, Switzerland

Francesca Genuzio − *Elettra-Sincrotrone Trieste S.C.p.A., 34149 Trieste, Italy;* Present Address: IOM-CNR, Laboratorio TASC, S.S.14-km 163.5 km in Area Science Park, Basovizza, 34149 Trieste, Italy; orcid.org/0000-0003-0699-2525

Tevfik Onur Menteş − *Elettra-Sincrotrone Trieste S.C.p.A., 34149 Trieste, Italy*

Andrea Locatelli − *Elettra-Sincrotrone Trieste S.C.p.A., 34149 Trieste, Italy;* orcid.org/0000-0002-8072-7343

Complete contact information is available at: https://pubs.acs.org/10.1021/acs.jpcc.3c08360

Notes

The authors declare no competing financial interest.

ACKNOWLEDGMENTS

We thank Patrick Zeller for programming the software tool already used in ref 30 for the analysis of spatial moiré frequencies.

REFERENCES

(1) Kuhlenbeck, H.; Shaikhutdinov, S.; Freund, H.-J. Well-Ordered Transition Metal Oxide Layers in Model Catalysis - A Series of Case Studies. *Chem. Rev.* **2013**, *113* (6), 3986−4034.

(2) Netzer, F. P. "Small and beautiful" - The novel structures and phases of nano-oxides. *Surf. Sci.* **2010**, *604* (5−6), 485−489.

(3) Libuda, J.; Freund, H. J. Molecular beam experiments on model catalysts. *Surf. Sci. Rep.* **2005**, *57* (7−8), 157−298.

(4) Vesselli, E.; Peressi, M. Nanoscale Control of Metal Clusters on Templating Supports. *Stud. Surf. Sci. Catal.* **2017**, *177*, 285−315.

(5) Chen, M. S.; Goodman, D. W. Ultrathin, ordered oxide films on metal surfaces. *J. Phys.: Condens. Matter* **2008**, *20* (26), 264013.

(6) Burson, K. M.; Büchner, C.; Heyde, M.; Freund, H.-J. Assessing the amorphousness and periodicity of common domain boundaries in silica bilayers on Ru(0 0 0 1). *J. Phys.: Condens. Matter* **2017**, *29* (3), 035002.

(7) Yang, B.; Boscoboinik, J. A.; Yu, X.; Shaikhutdinov, S.; Freund, H.-J. Patterned Defect Structures Predicted for Graphene Are Observed on Single-Layer Silica Films. *Nano Lett.* **2013**, *13* (9), 4422−4427.

(8) Schroeder, T.; Hammoudeh, A.; Pykavy, M.; Magg, N.; Adelt, M.; Bäumer, M.; Freund, H. J. Single crystalline silicon dioxide films on Mo(112). *Solid-State Electron.* **2001**, *45* (8), 1471−1478.

(9) Weissenrieder, J.; Kaya, S.; Lu, J. L.; Gao, H. J.; Shaikhutdinov, S.; Freund, H. J.; Sierka, M.; Todorova, T. K.; Sauer, J. Atomic Structure of a Thin Silica Film on a Mo(112) Substrate: A Two-Dimensional Network of SiO_4 Tetrahedra. *Phys. Rev. Lett.* **2005**, *95* (7), 076103.

(10) Yu, X.; Yang, B.; Anibal Boscoboinik, J.; Shaikhutdinov, S.; Freund, H.-J. Support effects on the atomic structure of ultrathin silica films on metals. *Appl. Phys. Lett.* **2012**, *100* (15), 151608.

(11) Altman, E. I.; Götzen, J.; Samudrala, N.; Schwarz, U. D. Growth and Characterization of Crystalline Silica Films on Pd(100). *J. Phys. Chem. C* **2013**, *117* (49), 26144−26155.

(12) Kremer, G.; Alvarez Quiceno, J. C.; Lisi, S.; Pierron, T.; González, C.; Sicot, M.; Kierren, B.; Malterre, D.; Rault, J. E.; Le Fèvre, P.; Bertran, F.; Dappe, Y. J.; Coraux, J.; Pochet, P.; Fagot-

https://doi.org/10.1021/acs.jpcc.3c08360
J. Phys. Chem. C 2024, 128, 7235−7241

Revurat, Y. Electronic Band Structure of Ultimately Thin Silicon Oxide on Ru(0001). *ACS Nano* **2019**, *13* (4), 4720−4730.
(13) Navarro, J. J.; Tosoni, S.; Bruce, J. P.; Chaves, L.; Heyde, M.; Pacchioni, G.; Roldan Cuenya, B. Structure of a Silica Thin Film on Oxidized Cu(111): Conservation of the Honeycomb Lattice and Role of the Interlayer. *J. Phys. Chem. C* **2020**, *124* (38), 20942−20949.
(14) Xu, J.; Mu, C.; Chen, M. Structure and Properties of Ultrathin SiO_x Films on Cu(111). *Langmuir* **2022**, *38* (37), 11414−11420.
(15) Ruiz, I.; Wang, W.; George, A.; Ozkan, C. S.; Ozkan, M. Silicon Oxide Contamination of Graphene Sheets Synthesized on Copper Substrates via Chemical Vapor Deposition. *Adv. Sci., Eng. Med.* **2014**, *6* (10), 1070−1075.
(16) Li, J.; Zhuang, J.; Shen, C.; Tian, Y.; Que, Y.; Ma, R.; Pan, J.; Zhang, Y.; Wang, Y.; Du, S.; Ding, F.; Gao, H.-J. Impurity-induced formation of bilayered graphene on copper by chemical vapor deposition. *Nano Res.* **2016**, *9* (9), 2803−2810.
(17) Lisi, N.; Dikonimos, T.; Buonocore, F.; Pittori, M.; Mazzaro, R.; Rizzoli, R.; Marras, S.; Capasso, A. Contamination-free graphene by chemical vapor deposition in quartz furnaces. *Sci. Rep.* **2017**, *7* (1), 9927.
(18) Al-Kamiyani, S.; Mohiuddin, T. Improved control in elimination of white impurities on graphene by chemical vapor deposition (CVD). *AIP Adv.* **2018**, *8* (12), 125325.
(19) Ge, X.; Zhang, Y.; Chen, L.; Zheng, Y.; Chen, Z.; Liang, Y.; Hu, S.; Li, J.; Sui, Y.; Yu, G.; Jin, Z.; Liu, X. Mechanism of SiOx particles formation during CVD graphene growth on Cu substrates. *Carbon* **2018**, *139*, 989−998.
(20) Reckinger, N.; Tang, X.; Joucken, F.; Lajaunie, L.; Arenal, R.; Dubois, E.; Hackens, B.; Henrard, L.; Colomer, J. F. Oxidation-assisted graphene heteroepitaxy on copper foil. *Nanoscale* **2016**, *8* (44), 18751−18759.
(21) Jin, S.; Huang, M.; Kwon, Y.; Zhang, L.; Li, B.-W.; Oh, S.; Dong, J.; Luo, D.; Biswal, M.; Cunning, B. V.; Bakharev, P. V.; Moon, I.; Yoo, W. J.; Camacho-Mojica, D. C.; Kim, Y.-J.; Lee, S. H.; Wang, B.; Seong, W. K.; Saxena, M.; Ding, F.; Shin, H.-J.; Ruoff, R. S. Colossal grain growth yields single-crystal metal foils by contact-free annealing. *Science* **2018**, *362* (6418), 1021−1025.
(22) Zhang, J.; Lin, L.; Jia, K.; Sun, L.; Peng, H.; Liu, Z. Controlled Growth of Single-Crystal Graphene Films. *Adv. Mater.* **2020**, *32* (1), 1903266.
(23) Kratky, T.; Leidinger, P.; Zeller, P.; Kraus, J.; Genuzio, F.; Jugovac, M.; Sala, A.; Menteş, T. O.; Locatelli, A.; Günther, S. The fate of CVD grown graphene on copper: adsorbates, intercalates, and the role of released silicon from the reactor wall, Submitted, **2023**.
(24) Locatelli, A.; Aballe, L.; Mentes, T. O.; Kiskinova, M.; Bauer, E. Photoemission electron microscopy with chemical sensitivity: SPELEEM methods and applications. *Surf. Interface Anal.* **2006**, *38* (12−13), 1554−1557.
(25) Menteş, T. O.; Zamborlini, G.; Sala, A.; Locatelli, A. Cathode lens spectromicroscopy: methodology and applications. *Beilstein J. Nanotechnol.* **2014**, *5*, 1873−1886.
(26) Leidinger, P. Synthesis of supported and freestanding graphene: fundamental understanding of the reaction thermodynamics and kinetics on Cu. Ph.D. Thesis, Technical University Munich, Garching, 2022.
(27) Tanuma, S.; Shiratori, T.; Kimura, T.; Goto, K.; Ichimura, S.; Powell, C. J. Experimental determination of electron inelastic mean free paths in 13 elemental solids in the 50 to 5000 eV energy range by elastic-peak electron spectroscopy. *Surf. Interface Anal.* **2005**, *37* (11), 833−845.
(28) Apponi, A.; Convertino, D.; Mishra, N.; Coletti, C.; Iodice, M.; Frasconi, F.; Pilo, F.; Blaj, N. S.; Paoloni, D.; Rago, I.; De Bellis, G.; Cavoto, G.; Ruocco, A. Transmission through graphene of electrons in the 30 - 900 eV range. *Carbon* **2024**, *216*, 118502.
(29) Zeller, P.; Günther, S. What are the possible moiré patterns of graphene on hexagonally packed surfaces? Universal solution for hexagonal coincidence lattices, derived by a geometric construction. *New J. Phys.* **2014**, *16* (8), 083028.
(30) Tochihara, H.; Shirasawa, T.; Suzuki, T.; Miyamachi, T.; Kajiwara, T.; Yagyu, K.; Yoshizawa, S.; Takahashi, T.; Tanaka, S.; Komori, F. Scanning tunneling microscopic and spectroscopic studies on a crystalline silica monolayer epitaxially formed on hexagonal $SiC(000\bar{1})$ surfaces. *Appl. Phys. Lett.* **2014**, *104* (5), 051601.
(31) Zeller, P.; Ma, X.; Günther, S. Indexing moiré patterns of metal-supported graphene and related systems: strategies and pitfalls. *New J. Phys.* **2017**, *19* (1), 013015.
(32) Bauer, E. Multiple scattering versus superstructures in low energy electron diffraction. *Surf. Sci.* **1967**, *7* (3), 351−364.
(33) Xu, C.; Chen, G.; Zhao, Y.; Liu, P.; Duan, X.; Gu, L.; Fu, G.; Yuan, Y.; Zheng, N. Interfacing with silica boosts the catalysis of copper. *Nat. Commun.* **2018**, *9* (1), 3367.

https://doi.org/10.1021/acs.jpcc.3c08360
J. Phys. Chem. C 2024, 128, 7235−7241